Reduced In-Plane, Low Frequency Noise of an Active Flap Rotor

Ben W. Sim
UARC/AFDD
Ames Research Center
Moffett Field, California
ben.w.sim@us.army.mil

Ram D. JanakiRam
Flight Technology
The Boeing Company
Mesa, Arizona
ram.d.janakiram@boeing.com

Natasha L. Barbely
Aeromechanics Branch
NASA Ames Research Center
Moffett Field, California
Natasha.Barbely@nasa.gov

Eduardo Solis
Monterey Technologies, Inc.
Monterey, California
Eduardo.Solis@nasa.gov

ABSTRACT

Results from a recent joint DARPA/Boeing/NASA/Army wind tunnel test demonstrated the ability to reduce in-plane, low frequency noise of the full-scale Boeing-SMART rotor with active flaps. Test data reported in this paper illustrated that acoustic energy in the first six blade-passing harmonics could be reduced by up to 6 decibels at a moderate airspeed, level flight condition at advance ratio of 0.30. Reduced noise levels were attributed to selective active flap schedules that modified in-plane blade airloads on the advancing side of the rotor, generating counter-acting acoustic pulses that partially offset the negative pressure peaks associated with in-plane, steady thickness noise. These favorable reduced-noise operating states are a strong function of the active flap actuation amplitude, frequency and phase. The reduced noise levels resulted in reduction of predicted aural detection distance, but incurred vibratory load penalties due to increased hub shear forces.

INTRODUCTION

The ability to operate rotorcraft covertly is important in twenty-first century warfare. Rotorcraft offer strategic opportunities for mobile, close-in observation, support, and attack using either manned or unmanned mobile platforms. As such, stealth and acoustic discretions are prime considerations military helicopters must contend with for mission survivability. Tactical effectiveness of these airborne vehicles lies in their ability to remain concealed. In many ways, this is compromised by the use of lift-generating rotors that produce strong acoustic pressure disturbances (source noise). Low frequency rotor harmonic tones, emitted from near in-plane of the rotor, are particularly of concern[1], as they tend to propagate long distances without substantial reduction in strength from atmospheric absorption. As such, these low frequency harmonic tones are often responsible for early aural detection, which threaten operational survivability of helicopters.

Recent findings[2] at the U.S. Army Aerofightdynamics Directorate (AFDD), at Ames Research Center, have identified use of advanced rotor designs with active "on-blade" controls as a means to mitigate in-plane, low frequency noise. While methods such as Higher Harmonic Control[3] (HHC), Individual Blade Control[4] (IBC), active flap[5] and active twist[6] concepts have been systematically studied for many years, these efforts focused primarily on enhancing rotor performance, reducing vibration and suppressing strong blade-vortex interactions. Effectiveness of these methods lies in their ability to introduce cyclic variations, of two-per-rev or greater, to augment blade motions and blade airloads to achieve specific objectives. In a similar fashion, the noise mitigation approach recently proposed by AFDD[2] makes use of these active controls to modify inherent aerodynamic blade loads to generate an "anti-noise" waveform that offsets the low frequency sounds generated by the rotor. A separate study reported by the University of Maryland[7] also demonstrated the feasibility of achieving low frequency noise reductions using similar control strategies.

While this "anti-noise" approach has only been recently analytically studied and proposed, this paper serves, as a first of its kind, to highlight in-plane, low frequency noise reduction possibilities based on acoustic measurement obtained from a recent joint DARPA/Boeing/NASA/Army test[8] completed in April 2008 in the National Full-Scale Aerodynamic Complex's 40- by 80-Foot Wind Tunnel at Moffett Field, California. Of primary interest are results demonstrating the potential of using the Boeing-SMART active flap rotor to mitigate low frequency sounds radiating from near in-plane of the rotor. The extent of noise reduction will be reported in this paper as a function of single-harmonic active flap inputs (amplitude, frequency and phase). Significance of these findings for predicted perceived aural detectability and their implications/ limitations on platform applicability will also be discussed.

Presented at the American Helicopter Society 65th Annual Forum, Grapevine, Texas, May 27-29, 2009.

IN-PLANE, LOW FREQUENCY NOISE SOURCES & REDUCTION STRATEGY

Low frequency rotor harmonic noise originates from several different source mechanisms[9]. As depicted in Fig. 1a, one of these mechanisms is attributed to the displacement of surrounding fluid medium due to blade motion. As the blade moves in space, fluid particles in the medium are "pushed" by the moving blade surface causing acoustic waves to be radiated. This mechanism, first studied by Deming[10], is known as the "thickness" or monopole noise and presents itself as a large negative peak pressure that is a strong function of the advancing tip Mach number and airfoil geometry. Subsequent studies have shown that at sufficiently high advancing tip Mach numbers, delocalized (weak) shock-fronts are formed at the tips of the rotor blades, resulting in a nonlinear quadrupole phenomenon typically referred to as the "High-Speed Impulsive (HSI)" noise[9]. While HSI noise can dominate when it occurs, most helicopters today are designed to avoid operating in this region. Therefore, it is not considered in this present study.

The surface pressure distribution around the airfoil of a lifting rotor also contributes to the sound radiation field. In the absence of strong blade-vortex interaction[9], the resulting low frequency noise radiation is often referred to as steady loading noise[11] due to the inherent (steady) aerodynamic forces necessary to sustain flight. Conveniently, this mechanism can be decomposed into the out-of-plane loading (or the thrust) component and the in-plane loading (torque) component, with respect to the tip-path-plane of the rotor, as shown in Fig. 1a. At nominal rotor operating conditions, the out-of-plane loading component is typically dictated by large aerodynamic force associated with the rotor blade lift. On the other hand, in-plane loading component results from the vector sum of lift and non-viscous drag, and is usually much smaller in magnitude than its out-of-plane counterpart. Over the course of each revolution, these aerodynamic forces exert their influence on the surrounding fluid to create pressure waves that are radiated into the far-field as noise.

The net noise radiation is the linear sum of all the effects stated above and can be mathematically represented by the well-known Farassat's Formulation 1A (Eq. 1) for far-field noise radiation[12]. In this formulation, it is assumed that the rotor is operating below the delocalization Mach number and that contributions from the nonlinear quadrupole field are small. At low rotational Mach numbers, it is also often assumed that the surface pressures, at each span station, can be integrated along the chord-wise direction and be represented by a span-wise line of rotating point forces. This compact acoustic source approximation is valid when the wavelength of the radiated sound is much larger that the characteristic dimension of the source (blade chord) - a valid approximation here since we are only interested in long-wavelength, low frequency sound.

$$p'(\vec{x},t) = \int_{f=0}\left[\frac{\rho_o \dot{v}_n}{4\pi \cdot r \cdot (1-M_r)^2}\right]_{ret} dS \quad (Thickness) + \int_{f=0}\left[\frac{\dot{\ell}_i \hat{r}_i}{4\pi c_o \cdot r \cdot (1-M_r)^2}\right]_{ret} dS \quad (Loading) \qquad \text{(Eq. 1)}$$

Note that Eq. (1) is in the strictest sense a nonlinear integral equation that requires adding the contributions from all the discretized blade surface elements (of area dS) prescribed on a blade surface, $f = 0$. Often, the right-hand side integrals are assumed to be bounded, finite and basically independent of the left-hand side. The first right-hand side integral illustrates the thickness noise expression as a function of the surface velocity field normal to the blade (v_n). The second term shows the loading noise as a function of the chord-wise compact airload vector due solely to the surface pressure (l_i). It contains both out-of-plane component in the z-direction and in-plane component in the x-y plane. In both terms, acoustic radiation is fundamentally governed by the time rate-of-change of the controlling factors. Also, the source term integrands are weighted by the (1-M_r) Doppler factor and are also attenuated by the source-to-observer distance (r). The notation (c_o) denotes the speed of sound of the medium. According to Eq. (1), the radiated low frequency noise is simply a summation of the thickness and loading source terms taken at each retarded (source) time and correctly propagated and summed at the observer location (x) and time (t).

The nature and complexity of the source integrands render each mechanism's noise radiation directivity to be markedly different from each other. Figure 1b illustrates the far-field noise radiation patterns of the different mechanisms based on predicted values obtained from Eq. (1) for a typical helicopter at moderate-airspeed level flight cruise. The patterns are shown with normalized noise amplitude (based on the maximum level of each mechanism) at different observer elevation angle positions surrounding the rotor. In general, noise radiated forward of the rotor tends to be greater than noise radiated towards the rear due to Doppler amplification and higher advancing side tip Mach number. It is also evident that different observer positions receive different composition of sound. At positions near in-plane and forward of the rotor, the noise received is primarily due to thickness and in-plane loading mechanisms. This region is confined to about ±30° from the plane of the rotor. On the other hand, the rotor thrust mechanism (out-of-plane loading) dominates at locations out-of-plane. These observations are representative of typical lifting-rotor systems and hold true for most conventional single-rotor helicopters.

The presence of both a thickness source term and an in-plane loading term in the in-plane acoustic signature offers an interesting potential for noise cancellation. As discussed before, the two mechanisms originated from very different circumstances and can be treated as two independent source

events – thickness noise being solely due to fluid displacement associated with blade motion and geometry, whereas in-plane loading noise is a by-product of the surface pressure acting in the direction near in-plane of the rotor. The two mechanisms are, to first order, un-coupled and have no causality relationships

Because the directivity of the in-plane loading noise nearly matches that of thickness noise near in-plane of the rotor (Fig. 1b), there is a possibility of altering blade airload to generate an in-plane loading noise profile that would negate or reduce the thickness noise pulse (Fig. 2). Such an "anti-noise" profile must be of approximately the same shape and magnitude, but opposite in sign. Because most of the thickness noise energy resides in its strong negative peak, it implies that the resulting in-plane loading noise profile must contain a strong positive peak, and must be timed (phased) properly so that the peaks coincide to enable effective cancellation. As shown in a previous study[2], achieving this "anti-noise" profile requires an increase in the in-plane loading (in the drag direction) as the blade approaches the advancing side near 90° blade azimuth. This result is consistent with findings reported in Ref. 7, which illustrated that an increase in (in-plane) blade loading must be sustained throughout a range ±20° blade azimuth to attain a reasonable "anti-noise" profile that can properly negate the steady thickness noise pulse.

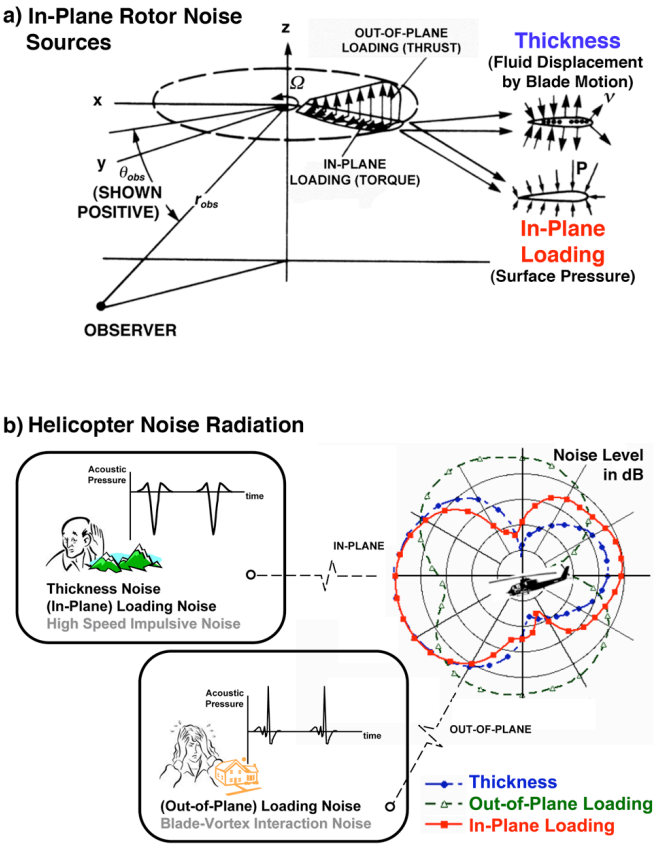

Figure 1. Helicopter noise radiation: a) source components, b) directivity characteristics

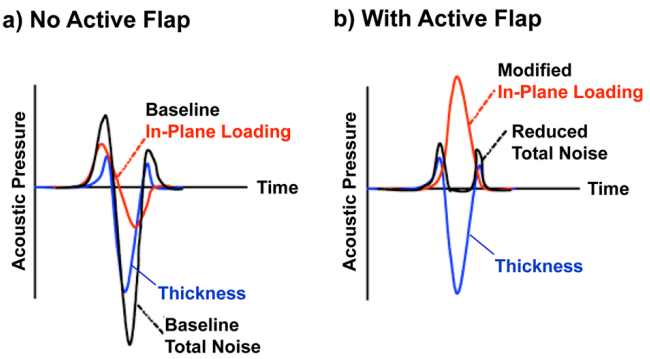

Figure 2. In-plane noise radiation: a) baseline, b) partial cancellation with modified in-plane loading noise

Based on these requirements, use of state-of-the-art active controls is deemed a good candidate for realizing such a goal. In most cases, these active control devices are embedded in the blade and/or the hub to enable temporal control of blade structural response and local aerodynamics. Additionally, from a noise perspective, these "on-blade" controls are more efficient than conventional active noise control (e.g. fuselage-mounted speaker arrays) in generating the required "anti-noise" pulse due to strong Doppler amplification resulting from high Mach number conditions near the blade tip.

BOEING SMART ROTOR TESTING

An opportunity arose in the early part of 2008 to validate the in-plane noise reduction strategy. Under a joint DARPA/NASA/Army-funded program, Boeing and a team from Air Force, NASA, Army, Massachusetts Institute of Technology, University of California at Los Angeles, and University of Maryland completed a wind tunnel test of the Smart Material Actuated Rotor Technology (SMART) rotor in the 40- by 80-Foot Wind Tunnel of the National Full-Scale Aerodynamic Complex (NFAC) at NASA Ames Research Center. The eleven-week wind tunnel test program[8] evaluated the forward flight characteristics of a full-scale active-flap rotor and quantified the effects of open- and closed-loop active-flap control on rotor loads, vibration, noise, and performance. The test demonstrated "on-blade" smart material control of flaps on a full-scale rotor for the first time in a wind tunnel with effectiveness and reliability of the flap actuation system, which was successfully demonstrated in more than 60 hours of wind tunnel testing.

Rotor Hardware

The SMART rotor (Fig. 3) is a 34-ft diameter, full-scale, bearingless, five-bladed main rotor modified from an existing MD900 Explorer rotor system. Each blade consists of HH-10 airfoil sections (12% thick) inboard and HH-06 airfoil sections (9.5% thick) outboard, with a linear twist of –10 degrees. The blade tip region, from 93% span station to the tip, has a parabolic leading edge sweep (22 degrees at the tip) with a 2:1 taper ratio. Nominal rotation speed of the

rotor is 392 RPM producing a tip speed of 695 ft/sec. At 5,811 lb thrust, the rotor thrust coefficient normalized by rotor solidity is 0.075 at sea level standard conditions.

Each blade contains an embedded piezoelectric actuator designed to drive a 18% span trailing-edge flap (located between 74% to 92% span station) at frequencies from two-per-rev (2P) up to six-per-rev (6P), with as much as 6 degrees amplitude authority, depending on the harmonic frequency. Inputs to the five blades are phased azimuthally such that each flap receives the same command at a given azimuth from a close loop (flap position) controller. Equation 2 shows the mathematical representation of a single-harmonically driven flap with deflection angle (δ_f) prescribed as a function of the blade azimuth (ψ), active flap amplitude (A_f), normalized harmonic frequency (H_f) and phase (ϕ_f). Positive deflection angles relate to flap down positions. For the rest of this paper, active flap settings will be described in a three-parameter form, $A_f/H_f/\phi_f$ – where A_f and ϕ_f are expressed in degrees and H_f is the normalized harmonic frequency expressed as integer multiples of the rotation frequency.

$$\delta_f = A_f \cdot \sin(H_f \psi + \phi_f) \qquad \text{(Eq. 2)}$$

Instrumentation

The Boeing-SMART rotor was mounted on the Large Scale Dynamic Rig (LSDR) when installed in the NFAC 40- by 80-ft test section (Fig. 4a). The LSDR consists of an upper and lower housing connected by a vertical stand strut. In the upper housing, the rotor hub is connected to a static mast, which was mounted to a five-component rotor balance. The static mast encloses the rotating drive shaft that transfers torque directly to the rotor hub. In addition, the upper fairing also encloses the balance housing and the hydraulic servo-actuators for the rotor/active flap control system. A vertical stand strut connects the upper balance housing to the lower housing that encloses the transmission and a 1,500-hp General Electric motor. The LSDR was mounted in the wind tunnel on a three-strut support system placing the rotor hub 23.7 ft above the tunnel floor at zero degree shaft tilt.

Rotor Characteristics

Rotor Blade	Modified MD900
Hub Type	Bearingless
No. of Blades	5
Blade Radius	203.1 inches
Rotor Speed	392 RPM
Tip Chord	10 inches
Airfoil	HH-10, HH-06
Twist	10 deg.

Trailing-Edge Flap Data

Radial Station	150 - 186 inches
Length	36 inches
Chord	3.5 inches
Hinge Location	75% Chord
Max. Flap Angle	± 6 deg.

Figure 3. Boeing-SMART rotor with active trailing-edge flap.

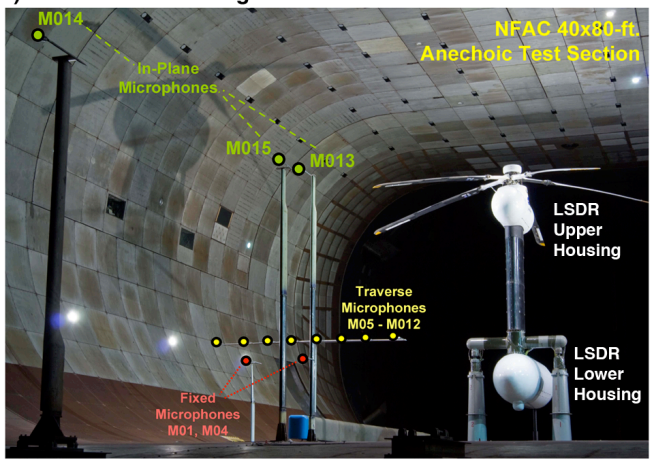

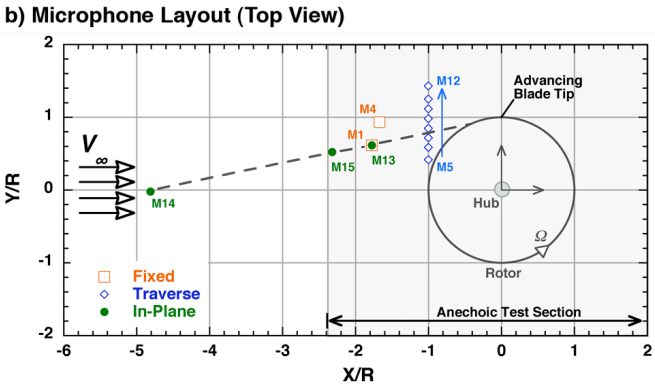

Figure 4. Test setup: a) Boeing-SMART rotor in wind tunnel, b) microphone layout.

For acoustic measurement, a set of microphones was strategically placed around the model to capture rotor noise sources of interest (Fig. 4a). These microphones were grouped into: a) out-of-plane fixed microphones (M1 and M4) to correlate to microphones used previously in the MDART test[13], b) traverse microphones (M5 through M12) that can be moved along guided rails for out-of-plane blade-vortex interaction noise mapping and c) in-plane microphones (M13, M15 and M14) for low frequency, in-plane rotor noise measurement. Microphones M13, M15 and M14 were mounted on tower struts to be near in-plane of the rotor (approximately 10 degrees below wind tunnel horizon). These microphones were also intentionally positioned along a straight line originating from the advancing blade tip to the tunnel centerline (Fig. 4b) to help determine near-field/far-field characteristics of in-plane rotor noise. With the exception of M14, all microphones are located within the acoustically-treated portion of the 40- by 80-Foot test section. Summaries of the microphone positions, relative to both the rotor hub center and to the advancing blade tip (both at zero shaft tilt), are illustrated in Tables 1a and 1b respectively.

Instrumentation-grade 1/2-inch free-field condenser microphones (G.R.A.S. Type 40AC) with nose cone fairings were used in the acoustic measurement. Microphone signals were pre-amplified at the source to minimize signal loss over the long wiring runs leading to a junction box housed below the test section - upon which the signals were sent to both an acoustic monitoring station and to the data acquisition console. Microphone gains were adjusted at the monitoring station on a per-test point, per-channel basis to maximize signal-to-noise ratio. In addition to the microphone signals, encoders on the rotor shaft provided a one-per-rev trigger signal, as well as a 256-per-rev and a 2048-per-rev sampling clock.

Table 1a. Hub-centered Microphone Positions

Mic. No.	XH, ft	YH, ft	ZH, ft	rH,ft	rH/R	ΨH, deg.	ΘH, deg.	
M1	-29.67	10.27	-17.94	36.16	2.14	160.9	-29.7	Fixed
M4	-27.92	15.59	-17.87	36.63	2.16	150.8	-29.2	
M5	-16.73	6.97	-15.13	23.61	1.39	157.4	-39.9	Traverse (ASA -200)
M6	-16.73	9.79	-15.13	24.59	1.45	149.7	-38.0	
M7	-16.73	12.02	-15.13	25.56	1.51	144.3	-36.3	
M8	-16.73	14.17	-15.13	26.64	1.57	139.7	-34.6	
M9	-16.73	16.42	-15.13	27.90	1.65	135.5	-32.8	
M10	-16.73	18.67	-15.13	29.28	1.73	131.9	-31.1	
M11	-16.73	20.90	-15.13	30.75	1.82	128.7	-29.5	
M12	-16.73	23.92	-15.13	32.88	1.94	125.0	-27.4	
M13	**-29.67**	**10.27**	**-5.34**	**31.85**	**1.88**	**160.9**	**-9.7**	In-Plane
M15	**-38.77**	**8.73**	**-7.13**	**40.38**	**2.39**	**167.3**	**-10.2**	
M14	**-80.36**	**-0.33**	**-14.84**	**81.72**	**4.83**	**180.2**	**-10.5**	

XH - Positive towards aft, YH - Positive towards starboard, ZH - Positive up

Table 1b. Advancing Blade Tip-centered Microphone Positions

Mic. No.	XA, ft	YA, ft	ZA, ft	rA,ft	rA/R	ΨA, deg.	ΘA, deg.	
M1	-29.67	-6.43	-17.94	35.26	2.11	192.2	-30.6	Fixed
M4	-27.92	-1.11	-17.87	33.17	1.99	182.3	-32.6	
M5	-16.73	-9.73	-15.13	24.57	1.47	210.2	-38.0	Traverse (ASA -200)
M6	-16.73	-6.91	-15.13	23.59	1.41	202.4	-39.9	
M7	-16.73	-4.68	-15.13	23.04	1.38	195.6	-41.1	
M8	-16.73	-2.53	-15.13	22.70	1.36	188.6	-41.8	
M9	-16.73	-0.28	-15.13	22.56	1.35	181.0	-42.1	
M10	-16.73	1.97	-15.13	22.64	1.36	173.3	-41.9	
M11	-16.73	4.20	-15.13	22.94	1.37	165.9	-41.3	
M12	-16.73	7.22	-15.13	23.68	1.42	156.7	-39.7	
M13	**-29.67**	**-6.43**	**-5.34**	**30.82**	**1.85**	**192.2**	**-10.0**	In-Plane
M15	**-38.77**	**-7.97**	**-7.13**	**40.22**	**2.41**	**191.6**	**-10.2**	
M14	**-80.36**	**-17.03**	**-14.84**	**83.47**	**5.00**	**192.0**	**-10.2**	

XA - Positive towards aft, YA - Positive towards starboard, ZA - Positive up

Data Acquisition

With the exception of wind tunnel condition and acoustics measurement, all rotor and active flap control data were recorded on Boeing's time-based sampling data acquisition system. For each test point, sixty-four revolutions of data (approximately 9.75 seconds) were collected to enable time-domain averaging on a rotor revolution basis. All channels, except those corresponding to acoustic measurement, were post-processed to 256 samples per revolution using the sampling clock from the rotor encoder. Acoustics data were separately acquired at a higher rate of 2048 samples per revolution, to capture the mid-to-high frequencies associated with human audible range. This azimuth-based sampling procedure isolates harmonic contents pertaining only to the rotation rate of the rotor, and suppresses all other un-wanted frequency contents, to achieve superior signal-to-noise ratio.

Acoustics Test Matrix

While the scope of the Boeing-SMART rotor test embodied a wide variety of flight conditions, in-plane rotor noise reduction was investigated only at a single operating condition at 123 knots level flight cruise (advance ratio of 0.30). At this condition, the nominal shaft tilt (un-corrected) was –9.11 degrees, with an advancing tip Mach number of 0.81 and a rotor thrust-to-solidity ratio of 0.075. Effects of active flap excitation were systematically studied via phase and amplitude sweeps at various active flap frequencies. A summary of the test points used in this paper and their corresponding operating conditions, is illustrated in Table 2. For all these cases, the rotor was trimmed to the desired thrust and zero blade-flapping moment, prior to active flap excitation, and was not re-trimmed during subsequent phase and amplitude sweeps.

Table 2. Acoustics Test Matrix

	Active Flap			Wind Tunnel Condition						Data Tracking		
	Af, deg.	Hf, P	ϕf, deg.	Tunnel Velocity, kt	Uncorr. Shaft Tilt, deg.	Advance Ratio	Rotational Tip Mach Number	Advancing Tip Mach Number	Thrust-to-Solidity Ratio	Boeing Event No.	NFAC Run No.	NFAC Point No.
Baseline				124.8	-9.11	0.299	0.622	0.808	0.07493	39.08300	57	68
2P Phase Sweep	1.5	2	0	124.8	-9.11	0.299	0.623	0.809	0.07427	39.07000	57	55
	1.5	2	30	124.8		0.299	0.623	0.809	0.07518	39.07100	57	56
	1.5	2	60	124.7		0.298	0.623	0.809	0.07605	39.07200	57	57
	1.5	2	90	124.9		0.299	0.623	0.809	0.07535	39.07300	57	58
	1.5	2	120	124.6		0.298	0.623	0.808	0.07492	39.07400	57	59
	1.5	2	150	124.7		0.298	0.623	0.809	0.07421	39.07500	57	60
	1.5	2	180	124.6		0.298	0.623	0.809	0.07455	39.07600	57	61
	1.5	2	210	124.6		0.298	0.623	0.809	0.07493	39.07700	57	62
	1.5	2	240	124.9		0.299	0.623	0.808	0.07621	39.07800	57	63
	1.5	2	270	124.9		0.299	0.622	0.808	0.07544	39.07900	57	64
	1.5	2	300	124.5		0.298	0.623	0.808	0.07651	39.08000	57	65
	1.5	2	330	124.8		0.299	0.623	0.808	0.07605	39.08100	57	66
	1.5	2	360	124.8		0.299	0.623	0.808	0.07599	39.08200	57	67
2P Amplitude Sweep	1	2	0	124.1	-9.11	0.298	0.623	0.810	0.07554	38.02700	55	27
	1.5	2	0	124.1		0.299	0.622	0.808	0.07344	38.02800	55	25
	2	2	0	124.3		0.299	0.623	0.809	0.07440	38.02600	55	26
3P Phase Sweep	1.5	3	0	124.0	-9.11	0.300	0.623	0.810	0.07571	33.03100	46	29
	1.5	3	30	123.6		0.299	0.623	0.809	0.07487	33.03200	46	30
	1.5	3	60	123.4		0.299	0.623	0.809	0.07441	33.03300	46	31
	1.5	3	90	123.9		0.300	0.623	0.809	0.07425	33.03400	46	32
	1.5	3	120	123.6		0.299	0.623	0.809	0.07353	33.03500	46	33
	1.5	3	150	123.1		0.298	0.623	0.809	0.07433	33.03600	46	34
	1.5	3	180	123.4		0.299	0.623	0.809	0.07605	33.03700	46	35
	1.5	3	210	123.8		0.300	0.623	0.810	0.07443	33.03800	46	36
	1.5	3	240	123.7		0.299	0.623	0.808	0.07465	33.03900	46	37
	1.5	3	250	123.4		0.298	0.623	0.808	0.07472	33.04700	46	45
	1.5	3	270	123.4		0.299	0.623	0.809	0.07505	33.04000	46	38
	1.5	3	300	123.3		0.298	0.623	0.809	0.07572	33.04100	46	39
	1.5	3	330	123.4		0.299	0.623	0.809	0.07600	33.04200	46	40
	1.5	3	360	123.5		0.299	0.623	0.809	0.07724	33.04300	46	41
3P Amplitude Sweep	1	3	250	124.2	-9.11	0.299	0.623	0.810	0.07517	38.02800	55	28
	1.5	3	250	123.4		0.298	0.623	0.808	0.07472	33.04700	46	45
	2	3	250	123.5		0.299	0.623	0.808	0.07319	33.04800	46	46
4P Phase Sweep	1	4	0	123.4	-9.11	0.300	0.623	0.809	0.07554	37.06500	54	36
	1	4	30	123.4		0.300	0.623	0.809	0.07588	37.06600	54	37
	1	4	60	123.1		0.298	0.623	0.809	0.07930	37.06700	54	38
	1	4	90	123.6		0.300	0.623	0.809	0.07839	37.06800	54	39
	1	4	120	122.8		0.298	0.623	0.809	0.07756	37.06900	54	40
	1	4	150	123.2		0.299	0.623	0.809	0.07788	37.07000	54	41
	1	4	180	123.2		0.299	0.623	0.809	0.07802	37.07100	54	42
	1	4	210	123.7		0.300	0.623	0.810	0.07578	37.07200	54	43
	1	4	240	123.4		0.299	0.623	0.809	0.07719	37.07300	54	44
	1	4	270	123.3		0.299	0.623	0.809	0.07791	37.07400	54	45
	1	4	300	123.5		0.300	0.623	0.810	0.07748	37.07500	54	46
	1	4	330	123.5		0.300	0.623	0.809	0.07854	37.07600	54	47
	1	4	360	123.2		0.299	0.623	0.809	0.07882	37.07700	54	48
4P Amplitude Sweep	0.7	4	180	124.5	-9.11	0.299	0.623	0.809	0.07748	38.02100	55	21
	1	4	180	123.9		0.299	0.623	0.809	0.07643	38.01900	55	19
	1.3	4	180	124.0		0.299	0.623	0.810	0.07685	38.02000	55	20

LOW FREQUENCY NOISE MEASUREMENT

Prior to the beginning of the Boeing-SMART rotor test, it was deemed necessary to re-examine the acoustic quality of low frequency sound measurement in the 40- by 80-ft test section. Modification of the 40- by 80-ft test section walls in 1997 with 42-inch deep acoustic liners reportedly improved and expanded aeroacoustics testing capabilities[14]. Subsequent post-mod calibration[15] reported superior sound absorption capabilities of 94% or more between 100 Hz and 2,500 Hz at most places in the test section. Unfortunately the frequency range examined did not extend to the lower frequency regimes that were of interest to the current Boeing-SMART rotor test – namely for the first three blade-passing harmonic tones at 32.7, 65.4 and 98.1 Hz.

A sound quality assessment was initiated in early January 2008 to evaluate how these low frequency harmonic tones propagate in an empty 40- by 80-ft test section under static, no-wind conditions. Using a calibrated sub-woofer, positioned at an equivalent location to the advancing blade tip of the Boeing-SMART rotor, acoustic measurements were obtained along a straight line that extended from the advancing blade tip position to the centerline of the tunnel (Fig. 4b). Audio tracks generated by a Matlab-based sound engine were played through the sub-woofer to simulate the dominant low frequency noise sources. This included harmonic pure tones corresponding to each of the blade-passing frequencies of the Boeing-SMART rotor and a mixed-harmonic audio track that combined multiple low frequency tones (first six blade-passing harmonics) to mimic helicopter noise. Obtaining noise measurements, at increasing distances from the sub-woofer source, provided valuable insights to the quality of sound measurement in the enclosed test section. Noise measurements must follow an inverse-distance decay law (i.e. 6 dB drop-off per doubling of distance) observed in a free-field environment if the acoustically-treated surfaces are truly anechoic. Any deviations from this free-field trend suggest the presence of facility-induced effects that can lead to inaccurate representation of the source noise.

A summary of the results obtained from this sound quality assessment effort is illustrated in Fig. 5. Relative sound pressure levels, at different frequencies, are plotted as a function of increasing distance from the sub-woofer sound source. Results for frequencies greater than 100 Hz appear to be consistent with findings reported in Ref. 15. Tonal sound decay with distance generally followed the 6 dB drop-off line, but showed oscillations of up to 3 dB within 40 feet of the sub-woofer source. As stated in Ref. 15, these fluctuations were attributed to non-uniform wall sound absorption characteristics in various parts of the test section. At distances beyond 40 feet (outside of the acoustically-treated portion of the test section), much larger oscillations on the order of 6 dB or greater were observed.

Similar trends were shown for the simulated helicopter noise signature with mixed-harmonic tones, but with smaller oscillation amplitudes up to 50 feet. These results imply that low frequency sound measurement at microphones M13 and M15 have relatively subdued facility effects and suggest the likelihood of adequate source noise representation at these locations (within an error band of ±2 dB). Unfortunately, as shown in Fig. 5, this does not hold true for the furthest microphone (M14), located 80 feet away outside of the acoustically-lined portion of the test section.

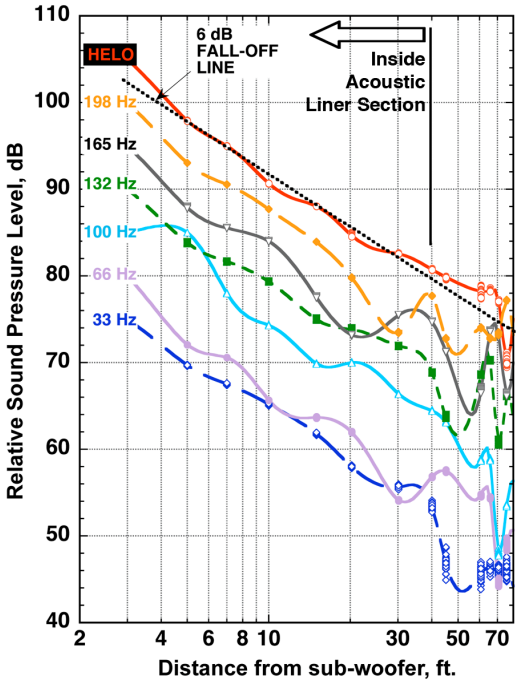

Figure 5. Low frequency sound assessment of NFAC 40- by 80-Foot Wind Tunnel test section.

Another factor that raises sound quality measurement concerns is the amount of ambient noise level present during "wind-on" conditions. Typically, ambient noise is dictated by the facility's fan drive system[16], but can include tonal/broadband sounds generated by hydraulic systems and flow-induced sounds from rotor test stand, wind tunnel surface or acoustics apparatus, such as microphone strut and/or microphone body. For all test data presented in this paper, the NFAC's variable-pitch fan-drive system operated at a fan speed of 115 RPM. Corresponding ambient noise levels measured at the three in-plane microphones (M13, M15 and M14) are indicated by the green lines in Fig. 6. These ambient noise levels were obtained at 123 knots wind speed, with a rotating bare hub (without blades) operating at 392 RPM nominal rotor speed. Compared to the Boeing-SMART rotor in baseline configuration (without active flap excitation), good signal-to-noise ratios of 18 dB or greater were observed for the two closer microphones M13 and M15. As shown in Fig. 6c, the far-upstream microphone M14 did not perform as well at certain blade-passing harmonics. It is also shown that microphone M14 could not replicate the source noise characteristics of the rotor, and will therefore be excluded from future discussions.

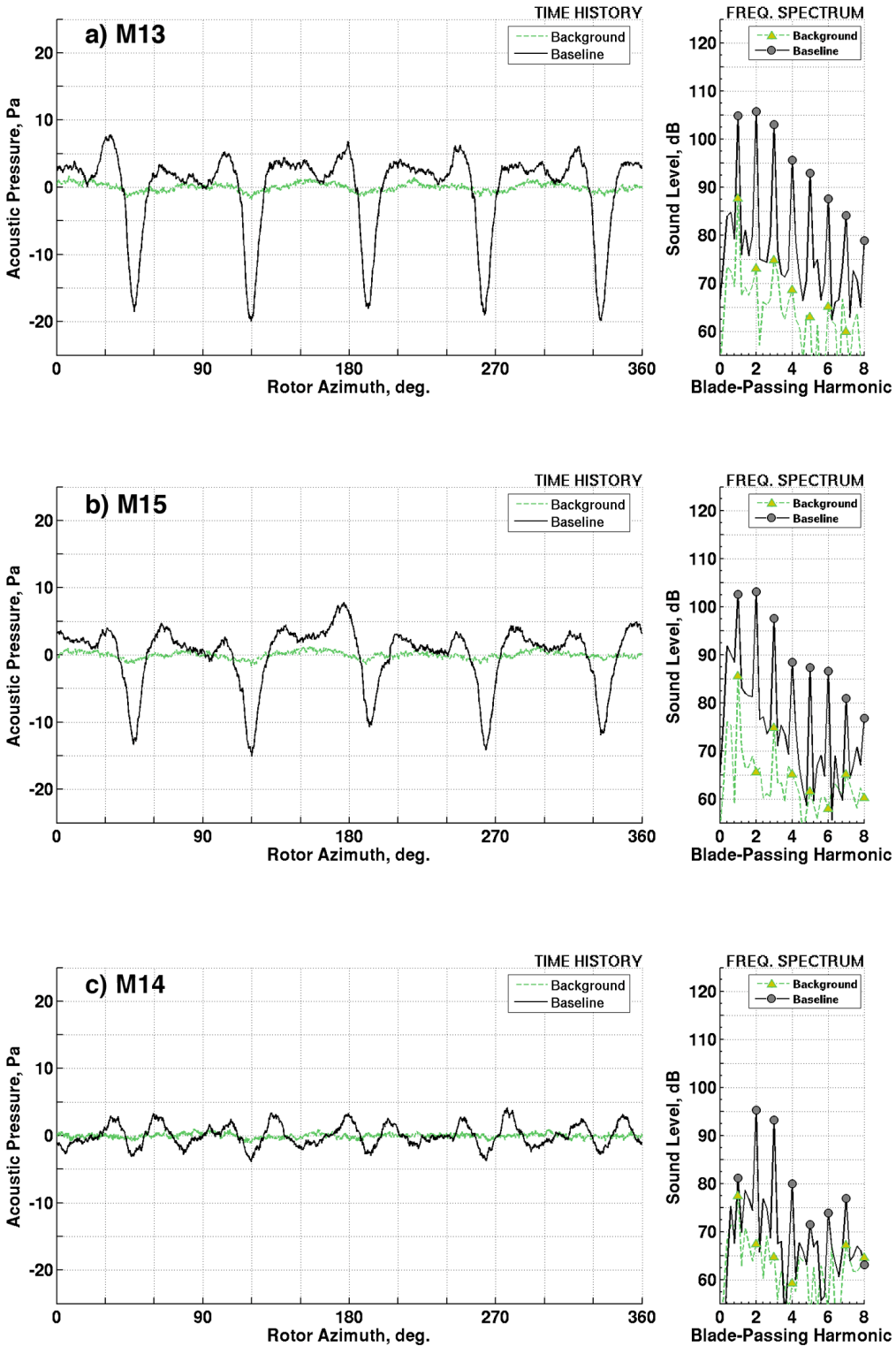

Figure 6. Rotor noise signal and ambient noise (64 revolutions) averaged time histories and corresponding frequency spectra at $\mu = 0.30$ for: a) M13, b) M15, c) M14.

Given the limitations of the facility, proximity of the installed microphones to the rotor is also a source of concern. Housing the full-scale Boeing-SMART rotor in the 40- by 80-Foot test section, with constraints imposed on microphones to be installed within the acoustically-treated section of the tunnel, challenges the ability to make accurate measurement representative of far-field external rotor noise radiation. Classical aeroacoustics theory stipulates that true far-field noise decays in an inversely-proportional manner with distance from its source. This implies that any distance-weighted acoustic metric must becomes invariant (with distance) in the far-field. Results in Fig. 7 for microphones M13 and M15, at baseline rotor configuration, demonstrate that this is indeed the case. Even though these microphones are no more than three rotor radii away from the advancing blade tip, distance-weighted acoustic time histories and spectral band levels showed similar amplitudes and features between the two microphones.

LOW FREQUENCY NOISE PREDICTIONS

In additional to noise data from wind tunnel measurement, predictions of low frequency sound for the Boeing-SMART rotor will be presented in this paper. Rotor noise predictions are derived from blade geometry and predicted blade airloads. The latter is obtained from comprehensive rotor analysis CAMRAD-II[17] using analytical modeling of the blade structural properties, rotor wake geometry, and local unsteady blade aerodynamics. Within the analysis, blade modeling is based on a series of span-wise distributed nonlinear beam finite elements. Each beam element is represented by a full range of blade motions, which includes axial, lead-lag, flapping and torsion. The trailing-edge flap is locally accounted for via span-wise changes in blade stiffness and blade mass properties. A non-uniform inflow model coupled to a free wake is used to obtain trimmed aerodynamic forces and blade motion solutions at a pre-defined rotor thrust and shaft tilt at zero blade-flapping.

In all ensuing calculations, the rotor blade is modeled using twenty aerodynamic panels on each blade and is evaluated at azimuth intervals of 15˚. The panels are more densely distributed at the outboard (tip) region of the rotor blade to accurately simulate the dominant region important for sound radiation. The relatively large time (azimuth) step is found to be adequate for capturing low frequency sound (up to six blade-passing harmonics) addressed in this paper. Steady airloads are computed using C-81 airfoil tables. Unsteady lift and moment in the attached flow are calculated based on compressible thin-airfoil theory. Provisions for modeling trailing-edge flap aerodynamics were incorporated via an extension of the airfoil tables to include flap angle as an input parameter. An empirically-based Mach number correction[18] is incorporated to better correlate to measured torsion and flap bending loads. This correction is applied only at the blade tip region (from 74% blade radius to the tip) to account for compressibility effects.

PSU-WOPWOP[19] is used to generate acoustics predictions reported in this paper. The code makes use of the blade geometry, and CAMRAD-II-derived blade motion and aerodynamic loading to resolve rotor acoustics radiation in the time domain. The acoustic equation, Farassat's Formulation 1A (Eq. 1), is implemented in PSU-WOPWOP to relate the aforementioned blade geometry and airloads to acoustic pressures at observers in both the near and the far-field. In this paper, PSU-WOPWOP is configured to simulate a single isolated rotor operating in a steady-state, wind tunnel environment. Only the linear thickness noise source and "on-surface" loading noise source terms are considered.

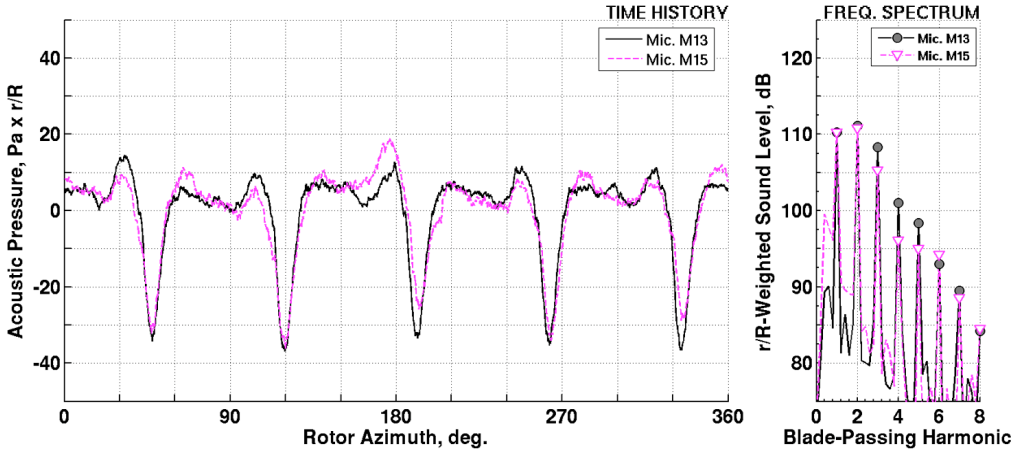

Figure 7. Near-field/far-field comparison of distance-weighted, averaged time histories and frequency spectra for microphone M13 and M15.

RESULTS & DISCUSSION

The following section reports findings from the Boeing-SMART rotor test during which the active flap was systematically excited to minimize low frequency, in-plane noise. Only results for single harmonic flap actuation are shown (as a function of flap, amplitude, frequency and phase) and are compared to baseline (no active flap actuation) conditions, to assess their potential for low frequency, in-plane noise mitigation. All of the ensuing results correspond to level flight cruise at 0.30 advance ratio (Table 2) and are reported solely based on microphone M13 measurements, even though similar findings were observed for microphone M15 as well.

Baseline configuration

Figure 8 shows the sixty-four revolution-averaged acoustic time history and frequency spectra (for the first eight blade-passing harmonics) measured for the baseline configuration (with no active flap) at microphone M13. Over the course of one rotor revolution from 0˚ to 360˚ rotor azimuth, five distinct pulses manifest in the time history – each owing to a different blade on the five-bladed Boeing-SMART rotor system. A large negative pressure peak dominates each pulse. As discussed before, this is primarily attributed to the thickness noise mechanism associated with blade/airfoil geometry rotating at moderate-to-high Mach numbers. Although not explicitly shown, there is a smaller contribution from loading noise mechanism due to in-plane, chord-wise blade forces, that accounts for approximately one-third of the acoustic energy[7] at this advancing tip Mach number.

From the same figure, it is also evident that in-plane noise radiation of the Boeing-SMART rotor is dominated by relatively large pulse-width, hence low frequency, negative thickness noise peaks – with very little mid-to-high frequency content commonly associated with impulsive rotor noise mechanisms, such as blade-vortex interactions. At 109.76 dB, the low frequency sound pressure level (LFSPL) noise metric, which embodies acoustic energy only in the first six blade-passing harmonics, is of comparable magnitude with the full-spectrum energy level depicted by the overall sound pressure level (OASPL). A mid-frequency sound pressure level (MFSPL) indicator, which accounts for higher frequencies, greater than sixth blade-passing harmonic, shows a magnitude that is 20 dB smaller. Naturally, this implies that in-plane noise of the Boeing-SMART rotor, at this operating condition, is dominated by lower frequencies associated with lower blade-passing harmonic tones.

Predictions from CAMRAD-II/PSU-WOPWOP are shown to be in excellent agreement with measurement. Gross features of the acoustic time history, and in particular, the negative peak pressures, are well simulated for the baseline configuration with no active flap excitation. Predicted spectral band levels show less than 2 dB differences, compared to measured values, for the first eight blade-passing harmonics.

Single harmonic flap input: Phase sweep

Figure 9 illustrates the effects of operating the active flap at two-, three- and four-per-rev (2P, 3P and 4P) separately, as a function of input phase angles depicted on the x-axis. At 2P and 3P settings, the active flap was commanded to deliver a flap deflection of 1.5˚; whereas, only a 1.0˚ flap amplitude was realized at 4P due to high blade loads. Changes in LFSPL decibel levels at microphone M13 (from baseline value) are plotted on the y-axis with negative decibel numbers indicating reduction in noise levels.

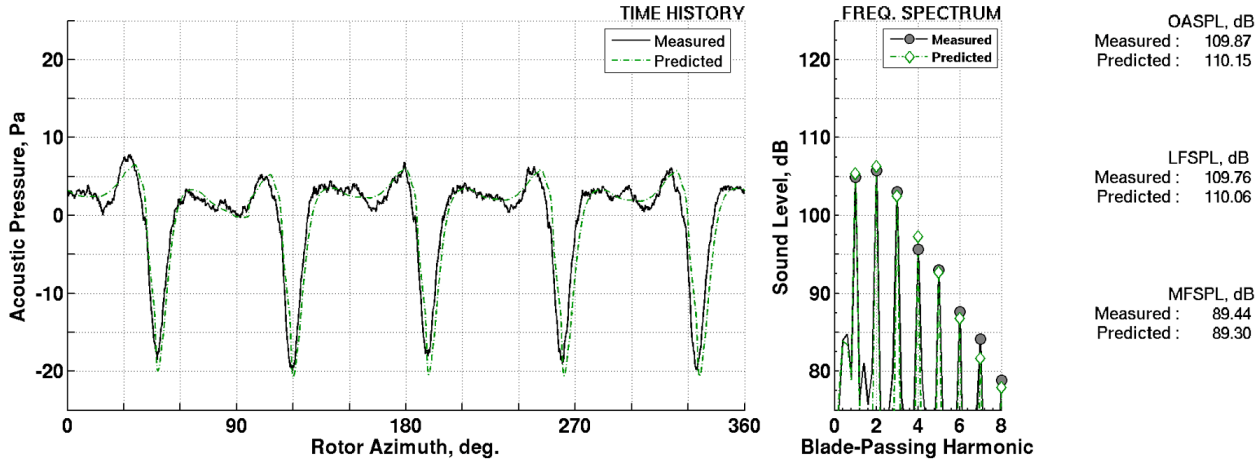

Figure 8. Measured and predicted acoustic time histories and frequency spectra for baseline condition (microphone M13).

Figure 9 reveals that low frequency noise at microphone M13 varies with input phase setting during single harmonic flap actuations. While a majority of these settings increased noise, there were certain phase inputs that resulted in noise reductions. Note that each active flap frequency setting resulted in a somewhat different "best" phase angle that delivered the greatest amount of noise reduction. For 2P flap actuation, this "best" phase angle occurs at 0˚, while at 3P, it is shifted to 250˚, and at 4P is shifted to 180˚. The amount of low frequency noise reduction is also different at each of these frequencies: with 2.8 dB reduction at 2P, 4.5 dB reduction at 3P and 4.8 dB reduction at 4P. As will be shown in subsequent sections, these "best" phase angle values and their corresponding dB reductions trends are intrinsically related to changes in the blade aerodynamic forces and blade motions induced by the sinusoidally-oscillating flap.

Noise predictions for these phase sweep conditions are also shown in Fig. 9 and yield favorable comparisons with measured data. The general noise trends are well-captured, with predicted noise reduction amplitudes matching measured values to within ±3 dB. A slight discrepancy in the predicted "best" phase setting is noticed, which amounts to approximately 30˚ lag in phase for 2P and 4P cases, and about 10˚ lag at 3P. The reason for this phase lag is unknown, but it would suggests that existing comprehensive rotor analyses may not have sufficient fidelity to capture trailing-edge flap aerodynamics and/or resultant blade motions accurately.

Acoustic time histories for these measured and predicted "best" phase conditions are illustrated in Fig. 10. Compared to measured baseline noise, operating the active flap clearly suppresses strong negative pressure peaks that set the low frequency sound levels at microphone M13. For 3P and 4P flap settings, the measured negative peak pressures associated with each blade were reduced by almost 50%. Reductions in the measured spectral band levels were also observed, although not uniformly across all blade-passing harmonics. As discussed before, this phenomenon owed its origin to the active flap's ability to alter blade aerodynamics locally on the rotor where the dominant noise source originated. At these "best" phase conditions, an "anti-noise" pulse triggered at the right time was able to partially cancel the negative peak pressure. It is also shown that additional noise was introduced due to the prescribed sinusoidal flap motion that modified blade airloads at other locations on the rotor.

Predicted noise profiles demonstrated good correlation with measured negative peak pressures, in terms of both amplitudes and trends. Results from CAMRAD-II/PSU-WOPWOP were consistent in showing a smaller reduction in negative peak pressures for 2P active flap frequency and larger reductions for 3P and 4P. However, details of the time history predictions in the vicinity of the negative peak pressure seem to deviate from measurement. In particular, additional acoustic pressure fluctuations are predicted that led to higher spectral band levels beyond the fourth blade-passing harmonics compared to measurement. These discrepancies suggest the lack of modeling fidelity associated with higher harmonic blade motions and blade aerodynamic response induced by active flap excitations.

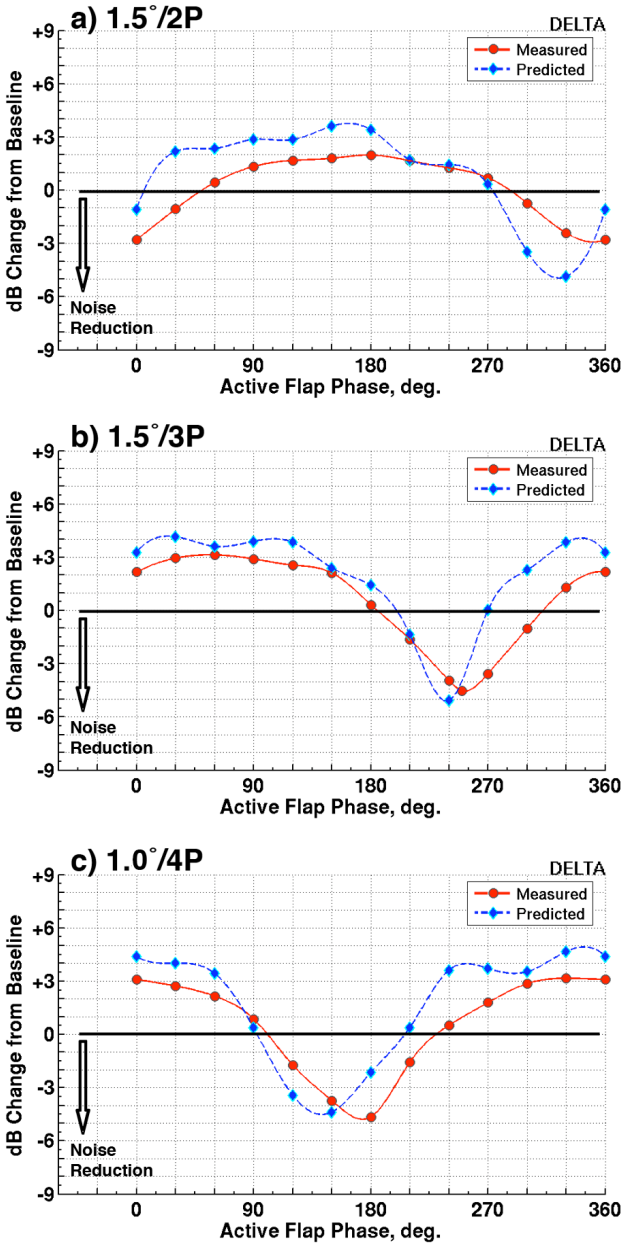

Figure 9. Changes in LFSPL (from baseline) at microphone M13 as a function of active flap phase input: a) 1.5˚/2P, b) 1.5˚/3P, c) 1.0˚/4P.

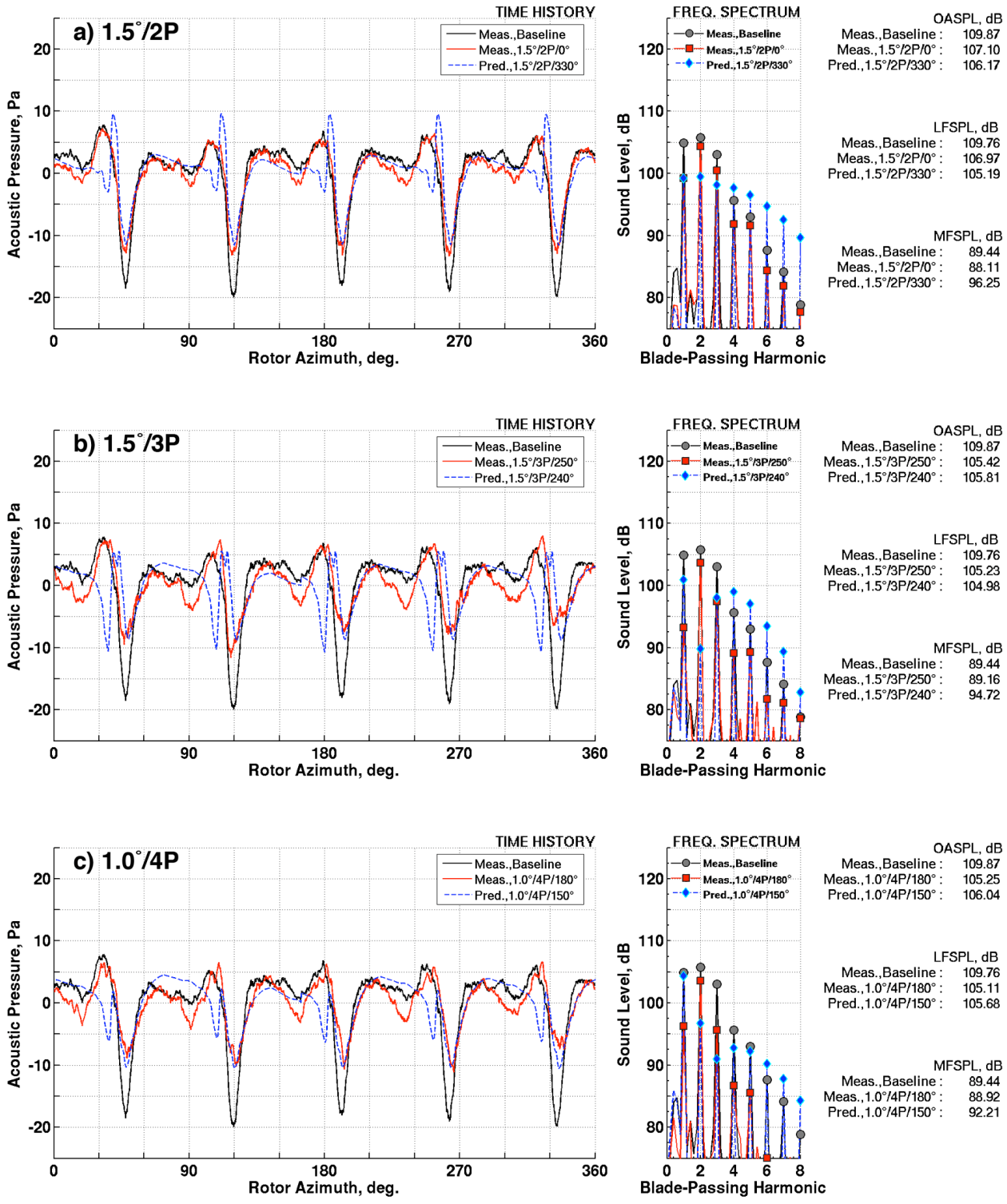

Figure 10. Acoustic time histories and frequency spectra at "best" phase conditions (microphone M13): a) 1.5°/2P, b) 1.5°/3P and c) 1.0°/4P.

The different "best" active flap phase settings at each frequency are governed by flap-induced blade response, and the resulting aerodynamic forces. Figure 11 illustrates measured active flap deflection for blade 1 on the advancing side of the rotor from 0˚ to 180˚ blade azimuth, where the peak negative pulse occurs[9]. These flap deflection plots are shown for the different "best phase" 2P, 3P and 4P flap actuation cases, along with blade torsion, flap-wise bending and chord-wise bending time histories at the 82% radial station corresponding to near mid-span of the active flap. For comparison purposes, similar time histories for baseline conditions, and for a "worst" phase setting, typically at 180˚ out-of-phase, are shown.

The most striking feature in Fig. 11 is the presence of a consistent active flap deflection trend (at source noise location from 90˚ to 110˚ blade azimuth for microphone M13) that governs when in-plane noise reduction occurs. All the "best" phase scenarios showed decreasing flap deflections with time (azimuth) – signifying that the active flap is moving from a flap down position (positive flap deflection) to a flap up position (negative flap deflection). This is found to be the case for the "best phase" cases at 2P, 3P and 4P flap activation frequencies. Note that the flap operated in the opposite manner for all the "worst" phase scenarios.

Similar observations are identified in measured oscillatory blade torsion response (with mean values removed). "Best" noise reduction consistently occurs when blade torsion (positive, pitch-up) increases with blade azimuth on the advancing side of the rotor near 90˚. Compared to the baseline, these measurements suggest that the blade tip region must be pitching nose-up to increase sectional angle-of-attack to impart favorable noise reduction. The opposite holds true for the "worst" phase scenarios where noise is amplified by the active flaps.

While it is difficult to identify the exact noise reduction mechanism solely based on blade torsion response measurements, previous analytical studies[2,7] have attributed reduced noise levels to an increase in the in-plane blade forces (positive towards trailing-edge) on the advancing side of the rotor. It was also shown from CAMRAD-II analyses[2] that active flap-induced aerodynamic forces and moments were responsible for altering the blade torsion response near 90˚ rotor azimuth. The net effect changes the local angle-of-attack at each span-wise station, and subsequently alters the in-plane force component via increased or decreased sectional lift. Sectional drag was shown to be relatively insensitive to these angle-of-attack changes and was determined not to be the primary cause of any in-plane force variations with harmonic flap motions.

A summary of these findings from Ref. 2 is depicted in Figs. 12 which illustrate how angle-of-attack changes associated with "best" and "worst" active flap actuations influence rotor blade in-plane force. During reduced noise operations, the resulting nose-up pitching moment between 90˚ and 110˚ blade azimuth causes the angle-of-attack to increase. This leads to progressively higher blade lift and increasing amount of in-plane force (Fig. 12a) that generates an "anti-noise" pulse with a positive peak pressure to cancel the negative thickness noise peak. The opposite effect is shown for the "worst" phase scenario with decreasing in-plane force associated with nose-down pitching moment and reduced angle-of-attack. The net (decreasing) in-plane force causes a negative loading noise peak pressure to be radiated that further reinforced the negative thickness noise peak. These findings are purely derived from analyses and have not been validated because of the lack of blade pressure instrumentations in the Boeing-SMART Rotor test.

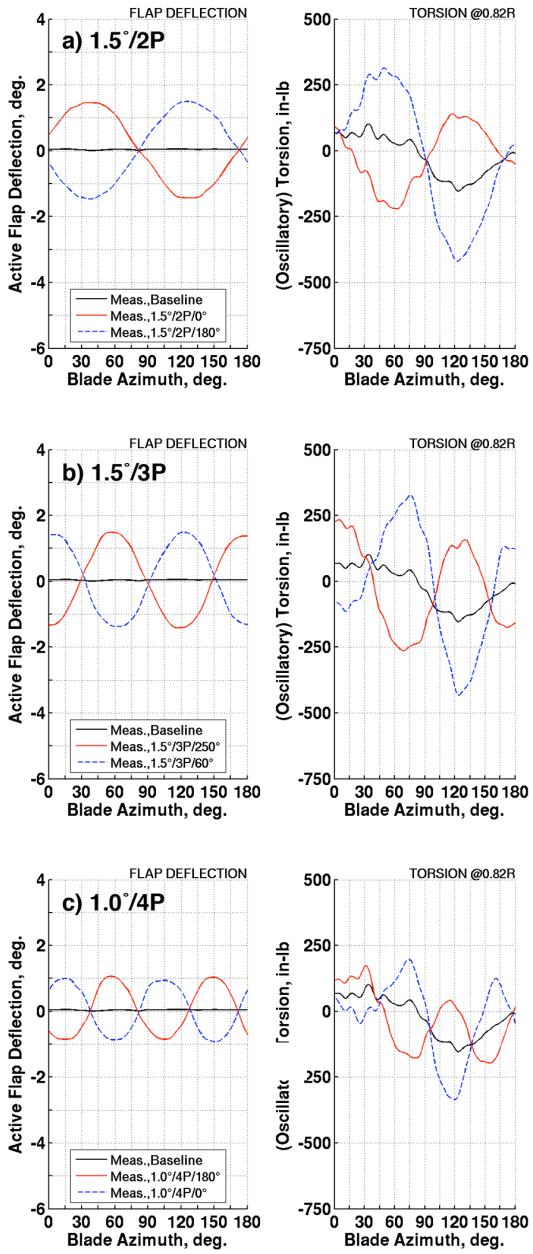

Figure 11. Measured (blade 1) flap deflection and blade torsion response (at 0.82*R*) for "best" and "worst" phase conditions: a) 1.5˚/2P, b) 1.5˚/3P and c) 1.0˚/4P.

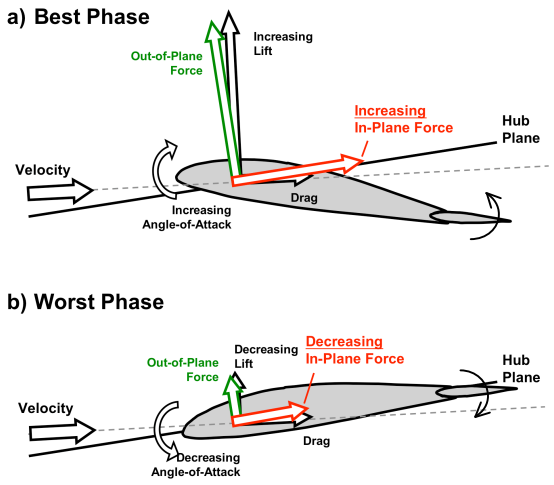

Figure 12. Effects of active flap on blade aerodynamic forces: a) "best phase", b) "worst phase".

Single harmonic flap input: Amplitude sweep

Amplitude sweeps of active flap deflections were also conducted during the wind tunnel test to explore further in-plane noise reduction possibilities. Figure 13 shows the results for 2P, 3P and 4P flap actuation where the active flap phase, at each frequency, was fixed at its "best" phase setting. Acoustic data for flap amplitudes ranging from 0.7˚ to 2.0˚ were collected, depending on rotor balance and blade load allowable tolerances. Within this range of flap amplitudes, Fig. 13 shows that increasing flap amplitudes at 3P and 4P achieved more noise reductions. Best noise reduction of 5.1 dB and 5.7 dB were obtained at 2.0˚ flap amplitude at 3P, and at 1.3˚ flap amplitude for 4P, respectively. Beyond these measured flap amplitudes, extrapolated trends suggest that there is an optimum point whereby further increase in flap amplitude does not necessarily result in more noise reductions. This is shown to be the case for 2P where noise reduction margin diminishes from 2.8 dB at 1.5˚ flap amplitude to 2.0 dB at 2.0˚ flap amplitude.

Predicted levels in Fig. 13 illustrate good correlation with measured data at small flap amplitudes up to 1.0˚. At larger flap amplitudes, discrepancies between predicted and measured noise reduction levels become more significant. An example is the 2P flap motion case that demonstrated up to 4.5 dB differences at about 2.0˚ flap amplitude (Fig. 13a). Similarly, predicted noise levels deviate from measurement by about 3 dB for the 4P case at the largest 1.3˚ flap amplitude setting.

Figure 14 illustrates the "best" phase, "best" amplitude measured acoustic time histories (microphone M13) for all the single harmonic flap actuation cases studied in this paper. Active flap excitation was found to reduce negative acoustic pressure peaks by at least 50%. These reductions, however, did not occur uniformly for the pulses emanating from all five blades. Compared to the baseline acoustic signature, and also to the more benign 2P case, actuating the trailing-edge flap at 3P and 4P appeared to generate much stronger blade-to-blade differences. In addition, these higher active flap frequencies also seem to incur higher MFSPL levels that denote added acoustic energy in the higher blade-passing harmonics.

For all these "best" phase, "best" amplitude cases, the flap deflection and blade response trends (Fig. 15) are consistent with those reported in the previous section (Fig. 11). With exception of chord-wise bending, it appears that steeper gradients in flap deflection, torsion and flap-wise bending (near 90˚ blade azimuth) result in higher levels of noise reduction. Although the reason is unknown, it is likely that these steeper gradients induce stronger temporal variations that generate "anti-noise" pulses of larger amplitude that cancel more of the negative pressure peak.

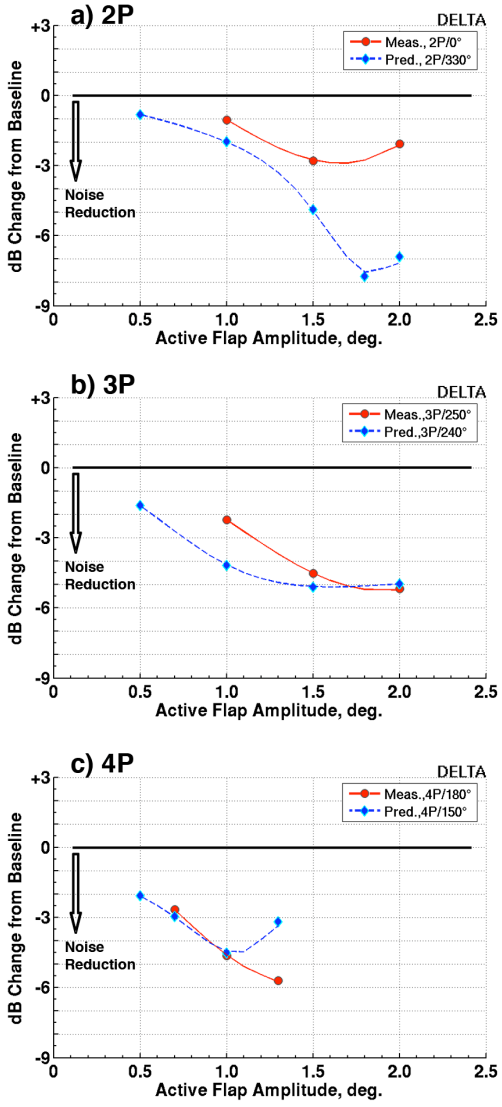

Figure 13. Changes in LFSPL (from baseline) at microphone M13 as a function of active flap amplitude.

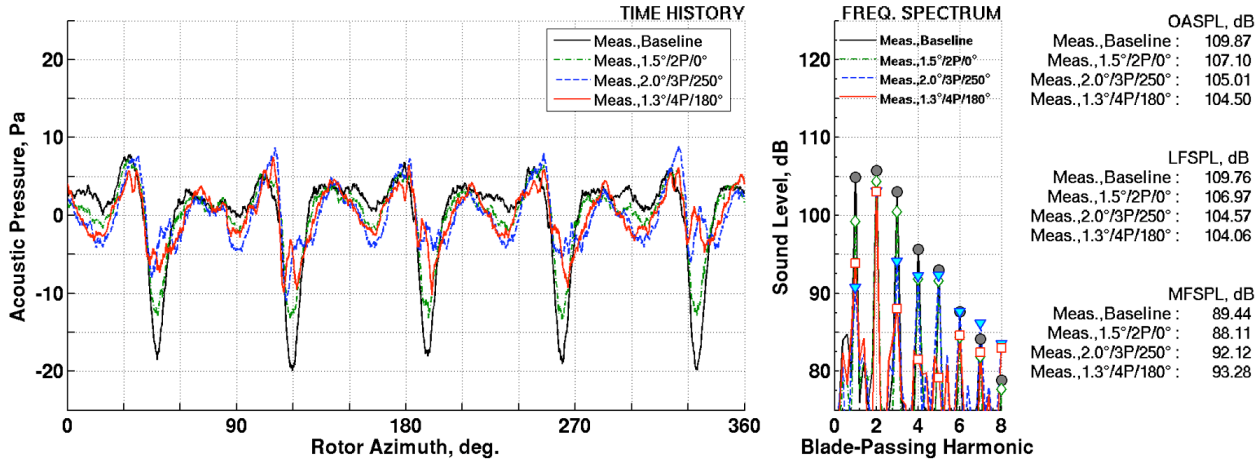

Figure 14. Measured acoustic time histories and frequency spectra at "best" phase, "best" amplitude conditions (microphone M13): a) 1.5°/2P/0°, b) 2.0°/3P/250°, c) 1.3°/4P/180°.

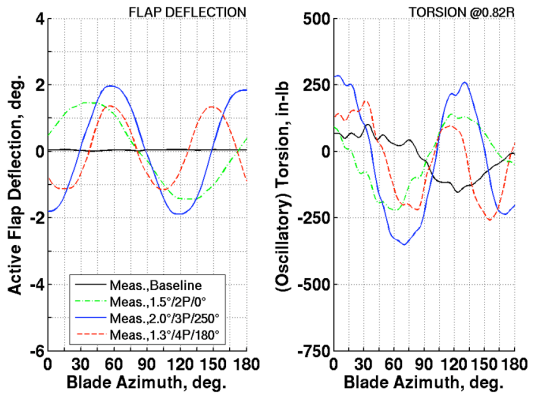

Figure 15. Measured (blade 1) flap deflection and blade response (at 0.82*R*) for "best" phase, "best" amplitude conditions: a) 1.5°/2P/0°, b) 2.0°/3P/250°, c) 1.3°/4P/180°.

cannot be replicated by 2P flap actuation with any reasonable active flap deflection amplitudes. These conflicting demands suggest the likelihood of a delicate compromise in the active flap actuation schedule (i.e. between "anti-noise" pulse-width and amplitude requirements) that would best suppress the baseline negative pressure peak.

Operating a single active flap at a single harmonic frequency also has limited use in achieving sound cancellation away from the negative pressure peaks. Spurious fluctuations are created off to the sides of the "anti-noise" positive pressure peak that added to baseline noise. This is largely in part due to active flap motions that were confined to harmonic cyclical deflections and not the time-varying deflections required to generate the exact and opposite "anti-noise" pulse.

IMPLICATIONS

The "anti-noise" profiles, generated by active flap motions, at microphone M13 are illustrated in Fig. 16. These profiles are calculated by subtracting the measured baseline time history from the "best" phase, "best" amplitude conditions shown in Fig. 14. Compared to baseline signature, single-harmonic active flap actuation at these amplitude/frequency/phase combination yielded carefully timed positive acoustic pressure peaks that resulted in suppression of the dominant negative pressure peaks associated with in-plane thickness noise. The synthesized "anti-noise" profiles are of similar pulse-width compared to baseline noise signature, with the 2P flap motion providing the broadest "anti-noise" best matched the baseline negative pressure peak. Gradual narrowing of the pulse-widths at 3P and 4P flap settings suggest that operating active flaps at higher frequencies may not be optimum in canceling the relatively wide negative pressure peak by any significant margins. However, as shown in Fig. 16, higher 3P and 4P flap frequencies yielded larger "anti-noise" amplitudes that

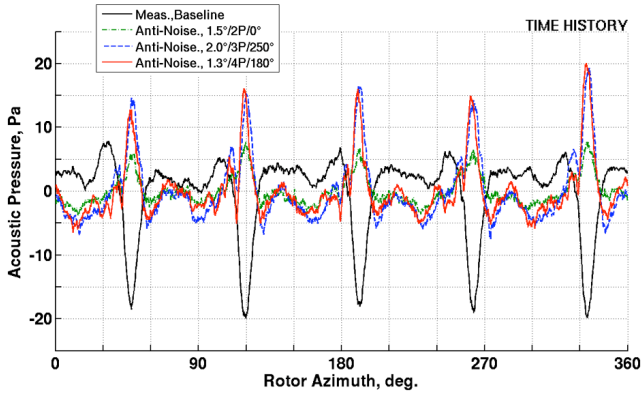

Figure 16. "Anti-noise" profiles (microphone M13) generated by "best" phase, "best" amplitude active flap conditions: a) 1.5°/2P/0°, b) 2.0°/3P/250°, c) 1.3°/4P/180°.

Reduction in (predicted) aural detection distance associated with these "best" phase, "best" amplitude cases are shown in Fig. 17. These calculations were obtained from the "I Can Hear It Now" (ICHIN) code[20] with source noise inputs derived from measured acoustic time histories shown in Fig. 14. Prior to implementation, the measured time histories were extrapolated to 500-feet and Doppler-shifted to simulate main rotor-only, flyover noise condition. Processed narrow-band spectral levels were subsequently fed into ICHIN to assess aural detection probability as a function of vehicle-to-observer distance and source frequency band. For all these cases, aural detection assessments were conducted with respect to standard low reference ambient noise, in an isothermal atmosphere of 70 degrees Fahrenheit, 70% relative humidity, and with zero cross-winds. A ground flow resistivity of 300 CGS Rayls, corresponding to loose soil condition, was used.

Figure 17a illustrates the ICHIN output for baseline condition. Horizontal bars indicating the probability of detection, and their accompanying distances (x-axis), are illustrated as a function of the source frequency band (y-axis). Longer bars depict less desirable circumstances where the vehicle can be detected further away. For simplicity, the overall aural detection metric is based on the largest predicted distance associated with 50% detection probability – which is 0.558 for the baseline case shown in Fig. 17a.

For the active flap cases illustrated in Fig. 17b through 17d, reduced in-plane, low frequency source noise is shown to directly reduce predicted detection distance. The best cases, at 3P and 4P (with approximately 5 to 6 dB low frequency noise reduction), enabled detection distance to be reduced by about 18%, while the 2P case (with 2.8 dB noise reduction) only provided 7%. It is also of interest to note that reduction in detection distance at lower frequencies for 3P and 4P, are accompanied by increases at higher frequencies. This is due to stronger mid-to-higher frequency source noise (MFSPL) generated as discussed before. Although not enough to set the overall detection distance here, it is likely to become an issue at higher frequency flap inputs.

The impact of reduced noise operations on rotor hub loads are illustrated in Fig. 18. For the three "best" phase, "best" amplitude conditions identified in this paper, reduction in in-plane noise and in predicted aural detection distance is accompanied by increased vibratory (five-per-rev) hub shear forces in both longitudinal (drag) and lateral (side) directions. Modified in-plane blade airloads resulting from active flap excitations are the most likely cause of this effect. In all three cases, increase in vibratory loads for both components are a function of the flap actuation frequency, with the highest penalty (290% increase from baseline) occurring in the longitudinal direction at 4P flap motion. This increase in vibratory hub loads is a cause for concern that should be studied further to quantify its significance and to mitigate any undesirable effects. Figure 18 also shows that the impact on measured vertical vibratory hub loads was much more benign than the longitudinal and lateral counterparts, and in some cases (2P and 3P) demonstrated slightly reduced hub loads compared to baseline. Although not shown, operating the active flap at these settings also incurred some impact on rotor performance. Details of this aspect of rotor operation are addressed in Ref. 8.

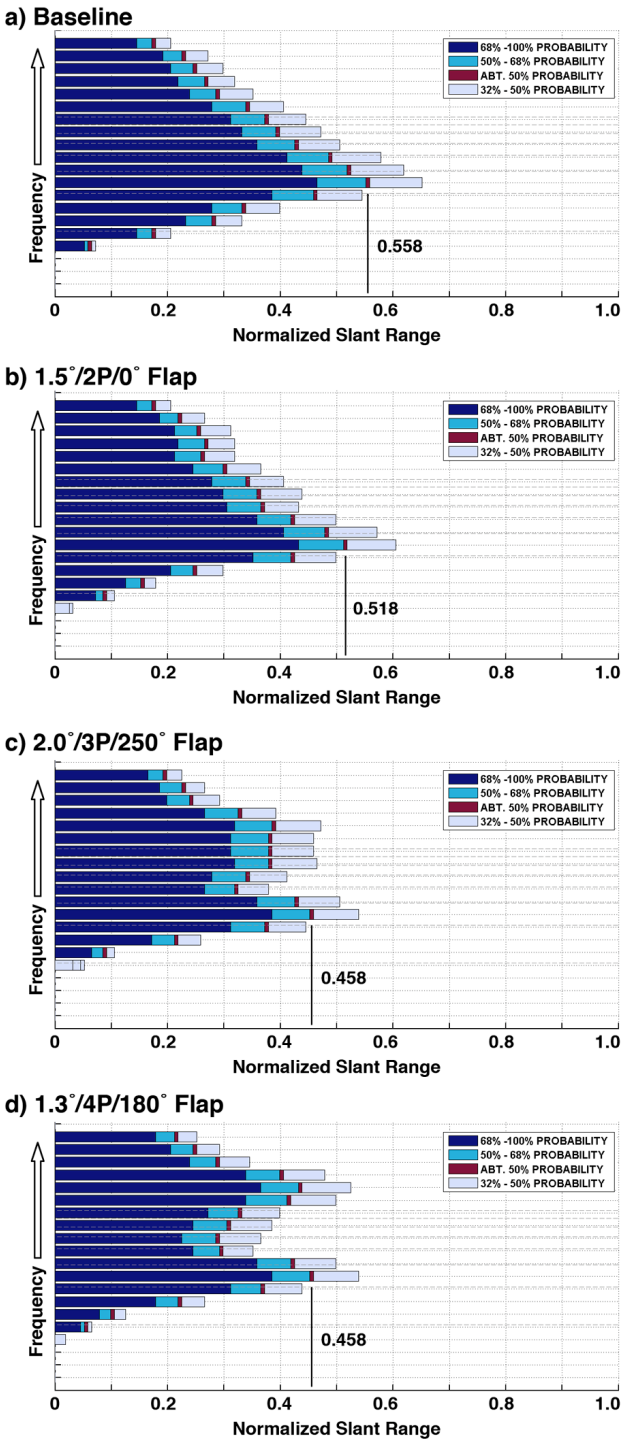

Figure 17. ICHIN results: a) Baseline, b) 1.5°/2P/0°, c) 2.0°/3P/250°, d) 1.3°/4P/180°.

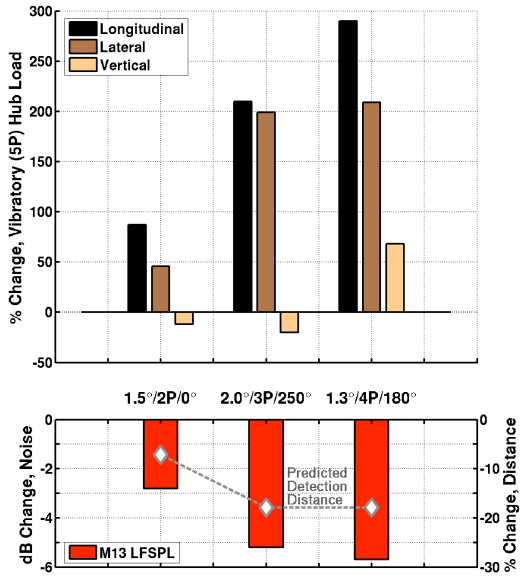

Figure 18. In-plane noise reduction implications on detection distance and rotor performance

OTHER LIMITATIONS & ISSUES

Aside from performance losses and increased vibratory hub loads, there are other limitations that question the ability of this noise reduction strategy to be applied in an advantageous and controlled manner.

Directionality issues

Directivity coverage is a concern, as the concept of reducing free-field noise via introducing an additional "anti-noise" source is known to be problematic. Tuning the active flap to reduce noise at one location is likely to increase noise elsewhere – generating local pockets of high and low noise levels where the "anti-noise" can either add or cancel the original source. Figure 19 illustrates this critical directionality issue via predicted noise level changes for a 1.0°/4P/150° active flap case in a local region ten rotor radii forward of the rotor. Changes in the low frequency sound pressure levels (LFSPL) from baseline are plotted in ±45° azimuth window from the forward station, and for –30° to 15° elevation angle with respect to the horizon. While the noise directly forward, in-plane of the rotor is shown to be reduced, it demonstrated also that higher noise levels can incur at other locations. The "hotspot" formed on the advancing side, near 140° azimuth, is an artifact of the single harmonic-driven flap introducing poorly phased "anti-noise" signatures that resulted in undesirable noise amplification at this location. In contrast, the second "hotspot" near 30° below the horizon is generated from local blade lift variations introduced by active flap excitation. As shown in Fig. 20 for the out-of-plane microphone (M1) for the 2.0°/3P/250° flap actuation schedule, this increase in noise over baseline can be rather significant. Naturally, these observations imply limited use of single-harmonic, single active flap actuation for global noise reductions.

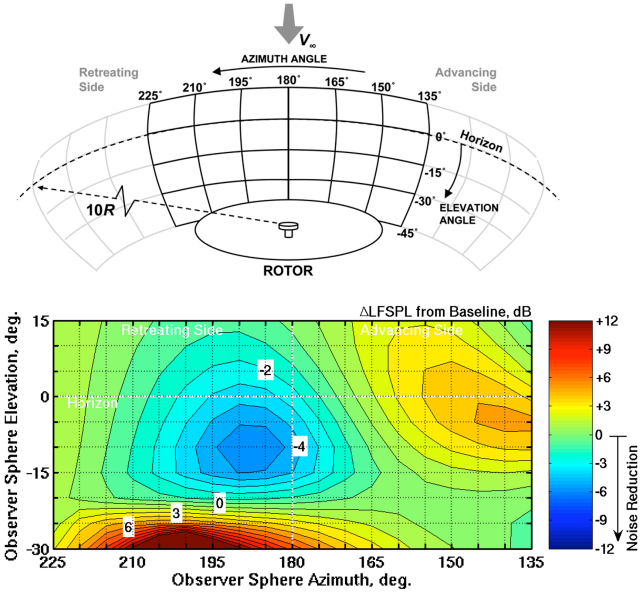

Figure 19. Predicted change in LFSPL from baseline at in-plane locations ten blade radii from the rotor.

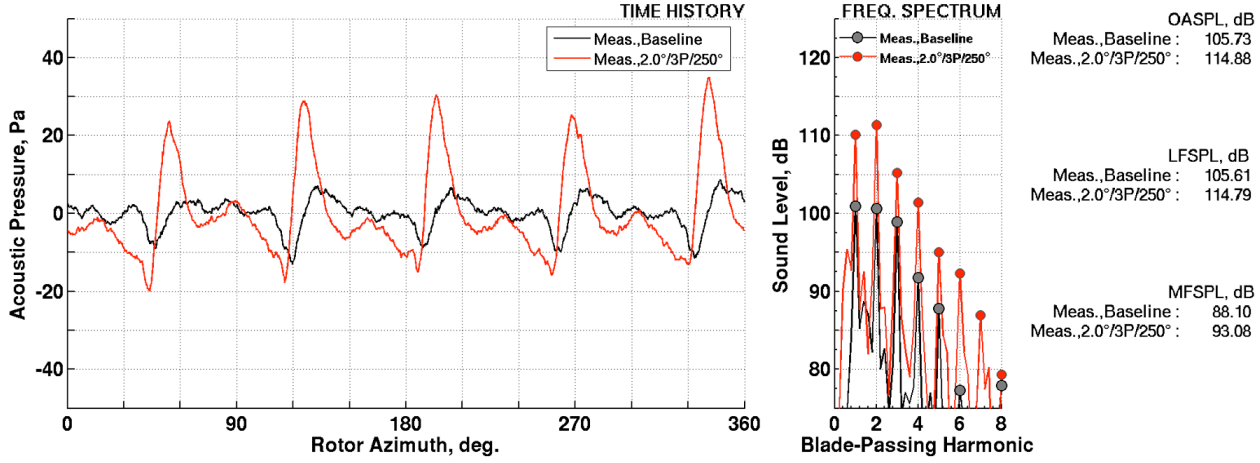

Figure 20. Measured acoustic time histories and frequency spectra at out-of-plane microphone (M1).

Feasibility across extended flight envelope

With measurement obtained at only one advance ratio (0.30) in this test, it is unclear if the Boeing-SMART active flaps are robust enough to deliver sufficient cancellation authority at higher airspeeds. The negative thickness noise peak increases considerably with airspeed, especially near delocalization Mach numbers[9], and would demand larger amplitudes and/or markedly different actuation strategies to generate the required "anti-noise".

IDEAL ACOUSTIC CONTROL

Although reduced in-plane, low frequency noise is demonstrated via the Boeing-SMART flap, the proposed noise cancellation concept is not limited to only this type of "on-blade" active control device. Based on present studies, anticipated demands for greater noise reductions, over a sufficiently wide area, calls for better "on-blade" controls and/or actuation strategies.

Foremost is the need for a control device that only affects in-plane (chord-wise) forces, and not the out-of-plane forces primarily associated with lift, to avoid increase in noise around the rotor. Use of multiple devices, distributed along the blade span, to enable better-phased and better "anti-noise" pulse shapes is highly desirable for larger noise reduction and for improved directionality considerations. In addition, it is beneficial to configure these devices to not operate at a single discrete harmonic frequency, but in a time-varying fashion that mimics the shape and form of the thickness noise pulse (with opposite sign). Doing so will likely allow for more complete and uniform cancellations across the low frequency bands and, simultaneously, minimizes noise residuals in higher frequencies.

Using a time-varying flap deflection controller can also provide additional means to suppress undesirable vibratory hub loads. A properly timed flap motion can be introduced on the retreating side of the rotor to generate opposing forces that minimize net hub forces. Ideally, this retreating side-only flap excitation can be tuned to counter-act vibratory hub loads caused by increased blade forces on the advancing side of the rotor. Although noise towards aft of the rotor will likely be increased, actuating the trailing-edge flap locally on the retreating side has negligible effects on the noise forward of the rotor due to Doppler directivity and, therefore, will not compromise any noise reductions obtained in front of the rotor.

CONCLUSIONS

Acoustic measurement obtained from the joint DARPA/Boeing/NASA/Army test in the National Full-Scale Aerodynamic Complex's 40- by 80-Foot Wind Tunnel demonstrated that it is possible to reduce in-plane, low frequency noise of the Boeing-SMART rotor via carefully chosen active flap deflection schedules. Results are shown for a condition corresponding to a level flight cruise at advance ratio of 0.30. Depending on the amplitude, frequency and phase of the (single harmonic) active flap excitation, up to 6 dB of noise reduction in the first six blade-passing harmonics at a single far-field microphone are reported. For the cases shown in this paper, best noise reduction is reported when the active flap was commanded at 1.3˚/4P/180˚.

The underlying mechanism of these reduced in-plane, noise levels is attributed to the ability of active flaps in generating appropriate "anti-noise" pulses that partially cancel the negative pressure peak commonly associated with steady thickness noise. It is surmised that these "anti-noise" are generated from increasing in-plane forces in the vicinity near the advancing side near 90˚ blade azimuth. This is achieved via increase in blade angle-of-attack associated with a (positive) noise up pitching moment caused by active flap actuations. The net increase in blade lift subsequently increases the in-plane force. These observations substantiated hypothesis and pre-requisites[2,7] , previously postulated, for achieving meaningful in-plane noise reduction.

Reduced in-plane, low frequency noise levels are shown to directly reduce aural detection distance through ICHIN analyses. A decrease of 18% in predicted detection distance was found to accompany source noise reductions of about 6 dB reported in this paper. ICHIN results also demonstrated the possibility of higher source noise frequency bands establishing aural detection distance with active flaps.

Higher hub shear forces are incurred during reduced in-plane noise operations. Engaging the active flaps with single-harmonic inputs reported in this paper resulted in up to 300% increase in longitudinal and lateral vibratory (five-per-rev) hub loads.

Conventional comprehensive rotor analysis and acoustic analogy-based codes are capable of providing good correlations with measured noise data at low flap amplitude settings. Predicted noise levels at higher flap deflections (greater than 1.0 degree) deviate from measured values in both amplitudes and trends.

Limitations of this noise reduction strategy, discussed in the paper, center on directivity concerns. Global noise reduction is not possible as the underlying physics of this approach relies on phase cancellation of steady thickness noise using modified loading noise generated by the active flaps. This yielded regions with high and low noise intensities that are indicative of constructive and destruction interference. Use of active flap is not necessarily best for reducing in-plane noise, primarily because it uses blade lift to achieve in-plane noise cancellation, but at the expense of generating more noise out-of-plane.

ACKNOWLEDGMENTS

Many thanks to the Boeing-SMART rotor test crew, including the participants from NASA Ames, Army/AFDD, Air Force/NFAC, M.I.T. and University of Maryland for enabling acquisition of the comprehensive acoustics database used in this study. In particular, the authors would like to thank:

- Dr. Friedrich Straub and Mr. Roger Smith (Boeing) for their helpful discussions on the SMART rotor,
- Mr. Cahit Kitaplioglu and Mr. Benton Lau (NASA Ames) for data collection and for their participation in acoustics calibration of the 40- by 80-Foot test section,
- Dr. Wayne Johnson (NASA Ames) for providing the CAMRAD-II calculations,
- Mr. Jan Van Aken and Ms. Lei Yang (NFAC) for developing the real-time acoustic post-processing software,
- Mr. Randall Peterson for consolidating the SMART rotor test database,
- Mr. Thomas Maier (AFDD), Mr. Malcolm Dinning (AATD) and Dr. William Warmbrodt (NASA Ames) for their encouragement and support on this research topic, and
- Prof. Fredric Schmitz (University of Maryland) for his elaborate discussions and insights on rotor acoustics.

REFERENCES

1. Crawford, C. Jr., "Noise Requirements from A Military Point of View," NASA CP-2052, May 1978, pp. 33-44.
2. Sim, B. W., "Suppressing In-Plane, Low Frequency Helicopter Harmonic Noise with Active Controls," American Helicopter Society San Francisco Bay Area Chapter's Aeromechanics Specialist's Meeting, Fisherman's Wharf, CA, January 2008.
3. Yu, Y., C. Tung, van der Wall, B., Pausder, H.-J., Burley, C., Brooks, T., Beaumier, P., Delrieux, Y., Mercker, E. and Pengel, K., "The HART-II Test: Rotor Wakes and Aeroacoustics with Higher-Harmonic Pitch Control (HHC) Inputs – The Joint German/French/Dutch/US Project," Presented at the American Helicopter Society 58th Annual Forum & Technology Display, Montreal, Canada, June 11-13, 2002.
4. Jacklin, S. A., Blaas, A., Teves, D., and Kube, R., "Reduction of Helicopter BVI Noise, Vibration and Power Consumption Through Individual Blade Control," American Helicopter Society 51st Annual Forum & Technology Display, May 1995.
5. Marcolini, M. A., Booth, E. R., Tadghighi, H., Hassan, A. A., Smith, C. D. and Becker, L. E., "Control of BVI Noise Using an Active Trailing-Edge Flap," American Helicopter Society San Francisco Bay Area Chapter's Vertical Lift Aircraft Design Conference, San Francisco, CA, January 1995.
6. Booth, E. R. Jr. and Wilbur, M. L., "Acoustic Aspects of Active-Twist Rotor Control," American Helicopter Society 58th Annual Forum & Technology Display, Montreal, Canada, June 11-13, 2002.
7. Gopalan, G. and Schmitz, F. H.,, "Far-Field Near In-Plane Harmonic Main Rotor Helicopter Impulsive Noise Reduction Possibilities," American Helicopter Society 64th Annual Forum & Technology Display, Montreal, Canada, April 29 – May 1, 2008..
8. Straub, F. K., Anand, V. R., Birchette, T., Lau, B. H., "Wind Tunnel Test of the SMART Active Flap Rotor," American Helicopter Society 65th Annual Forum and Technology Display, Grapevine, TX, May 27—29, 2009.
9. Schmitz, F. H., "Rotor Noise," Chapter 2 in book authored by Hubbard, H. H., *Aeroacoustics of Flight Vehicles, Theory and Practice, Vol. 1: Noise Sources*, Published for the Acoustical Society of America through the American Institute of Physics, 1995.
10. Deming, A. F., "Noise from Propellers with Symmetrical Sections at Zero Blade Angle, II., NACA TN-679, December 1938.
11. Gutin L., "On the Sound Field of a Rotating Propeller," NACA TM-1195, October 1948.
12. Farassat, F. and Succi, G. P., "The Prediction of Helicopter Rotor Discrete Frequency Noise," *Vertica*, Vol. 7, No. 4, pp. 309-320, 1983.
13. Jacklin, S. A., Lau, B. H., Nguyen, K. Q., Smith, R. L. and McNulty, "Full-Scale Wind Tunnel Test of the McDonnell Douglas Five-Bladed Advanced Bearingless Rotor: Performance, Stability, Loads, Control Power, Vibration and HHC Data," American Helicopter Society Aeromechanics Specialists Conference, San Francisco, California, January 19-21, 1994.
14. Schmitz, F. H., Allmen, J. R., and Soderman, P. T., "Modification of the Ames 40- by 80-Foot Wind Tunnel for Component Acoustic Testing for the Second Generation Supersonic Transport," NASA TM-108850, October 1994.
15. Soderman, P. T., Jaeger, S. M., Hayes, J. A. and Allen, C. S., "Acoustic Quality of the 40- by 80-Foot Wind Tunnel Test Section After Installation of a Deep Acoustic Lining," NASA TP-2002-211851, November 2002.
16. Allen, C. S., Jaeger, S. M. and Soderman, P. T., "background Noise Sources and Levels in the NASA Ames 40- by 80-Foot Wind Tunnel at the Turn of the Century: A Status Report," NASA TP-2003-212259, November 2003.
17. Johnson, W. R., "Rotorcraft Aerodynamics Models for a Comprehensive Analysis," American Helicopter Society 54th Annual Forum & Technology Display, Washington, D.C., May 1998.

18. Kottapalli, S. and Straub, F. K., "Correlation of SMART Active Flap Rotor Loads," American Helicopter Society 65th Annual Forum and Technology Display, Grapevine, Texas, May 27-29, 2009.

19. Shirey, J. S., Brentner, K. S., Chen, H.-N., "A Validation Study of the PSU-WOPWOP Rotor Noise Prediction System," 45th AIAA Aerospace Sciences Meeting and Exhibit, Reno, Nevada, January 8-11, 2007.

20. Mueller, A. W., Smith, C. D., LeMasurier, P., "Improvement of the Predicted Aural Detection Code ICHIN (I Can Hear It Now)," Noise-Con 93, pp. 403-408, May 1991.